PHILOSOPHICAL TRANSACTIONS OF THE ROYAL SOCIETY A MATHEMATICAL, PHYSICAL & ENGINEERING SCIENCES

Magnetic field–induced metal–insulator transitions in graphite and diluted magnetic semiconductors

Y. Iye

Phil. Trans. R. Soc. Lond. A 1998 **356**, 157-172
doi: 10.1098/rsta.1998.0155

Magnetic field-induced metal–insulator transitions in graphite and diluted magnetic semiconductors

By Y. Iye

Institute for Solid State Physics, University of Tokyo, Roppongi, Minato-ku, Tokyo 106, Japan

Two topical subjects related with the effect of magnetic field on electrical conduction and the metal–insulator transition are discussed. The first topic is an electronic phase transition in graphite, which is interpreted as a manifestation of a nesting-type instability inherent to a one-dimensional narrow Landau sub-band. The second topic is spin-dependent tranport in III-V based diluted magnetic semiconductors; in particular, a large negative magnetoresistance observed in the vicinity of metal–non-metal transition.

Keywords: graphite; field-induced transition; phase transition; magnetic semiconductors; magnetoresistance

1. Introduction

A strong magnetic field sometimes induces a fundamental change in the character of an electronic system. The effect is often manifested most dramatically in transport phenomena, which are governed by subtle combination and competition of various factors concerning the charge carriers and scatterers. Magnetic field affects the orbital motion (Landau quantization) on the one hand, and the spin state (Zeeman effect) on the other. The former effect is most distinct in high-mobility low-density electron systems, while the latter in systems with strong exchange interactions. In this paper, I discuss two subjects related to magnetic field effect on transport, each being an example of the respective category.

This paper consists of two parts. In the first half, a phenomenon called magnetic field-induced electronic phase transition in graphite is discussed. Although the phenomenon was discovered many years ago, we still do not have a clear understanding of what exactly is happening. I make an overview of the current status of our knowledge on this issue. In the second half, I present our recent results on III-V based diluted magnetic semiconductors, (Ga,Mn)As and (In,Mn)As. These materials with fairly high Mn concentrations were recently grown by molecular beam epitaxy, and were found to exhibit a variety of interesting magnetic and transport phenomena. I particularly focus on metal–insulator transition and a large negative magnetoresistance effect in (Ga,Mn)As systems.

2. Magnetic field-induced electronic phase transition in graphite

(*a*) *Graphite*

Graphite is a layered semimetal with low-density electrons and holes ($n = p \approx 10^{19}$ cm^{-3}) (Brandt *et al.* 1988). An electron pocket and two hole pockets are locat-

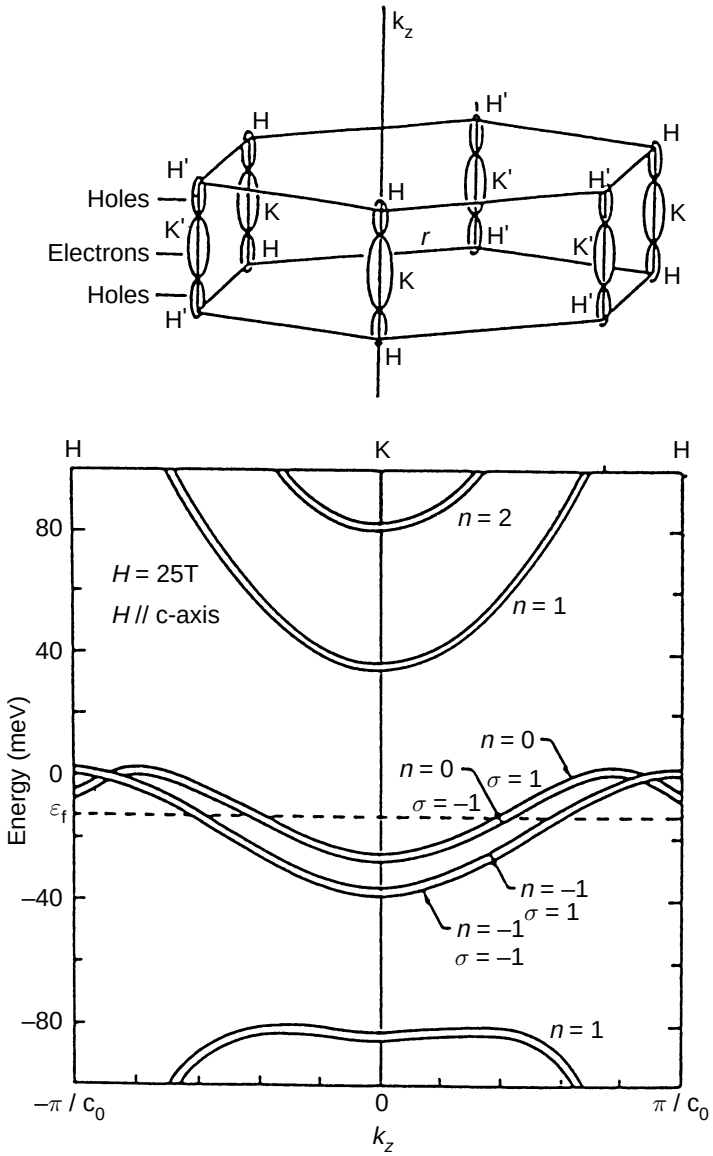

Figure 1. (Upper panel) Fermi surfaces of graphite. (Lower panel) Landau sub-band structure of graphite under magnetic field of 25 T applied parallel to the *c*-axis (normal to the layer plane).

ed along the vertical edge (*H*-*K*-*H*) of the hexagonal Brillouin zone as shown in the upper panel of figure 1. Due to the existence of two non-equivalent Brillouin zone edges, *H*-*K*-*H* and *H*′-*K*′-*H*′, these π bands have extra two-fold degeneracy in addition to the spin-degeneracy. The Fermi surfaces are much elongated in shape, which makes the in-plane effective mass very small ($m^* \approx 0.04m_0$) and the vertical mass large ($m^* \approx 10m_0$). The small in-plane mass and low carrier density conspire to drive the system in quantum limit at modest magnetic field applied parallel to the *c*-axis normal to the basal plane. The lower panel of figure 1 shows the Landau sub-band dispersion at $B = 25$ T, which is a typical field value for the phenomenon to be discussed (Iye *et al.* 1982).

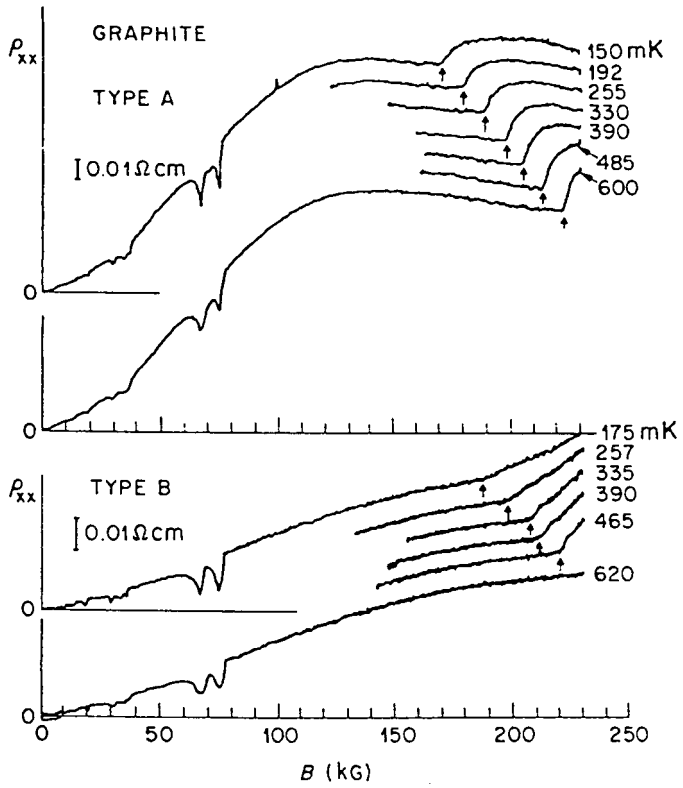

Figure 2. Magnetoresistance of graphite at different temperatures. Distinction between type-A and B is explained in the text.

In such high-fields, the in-plane orbital motion is quenched and we are left with the lowest spin-split electron and hole Landau levels, which form one-dimensional sub-bands with small bandwidth, $2|\gamma_2| \approx 38$ meV.

(*b*) *Magnetic field-induced electronic phase transition*

Figure 2 shows typical magnetoresistance curves at low temperatures (Iye *et al.* 1985). Type A signifies samples with minimal amount of ionized impurities, while type-B samples contain ionized impurities. Being a semimetal, graphite has a very large magnetoresistance ($\rho(B)/\rho(0)$ becomes of order at a few teslas). The zero-field resistivity is too small to be seen in this scale. The two dips around 7 T are the last Shubnikov–de Haas oscillations corresponding to the Fermi level crossing of the spin-split second lowest electron Landau levels. For the type-A sample, $\rho(B)$ increases approximately linearly with field up to *ca.* 10 T and tends to saturate at higher fields.

In the high-field range, an abrupt increase of resistance is seen. The field at which this occurs becomes lower with decreasing temperature. That the onset field strongly depends on temperature makes interpretation within a single-electron picture highly unlikely and suggests the many body origin of the phenomenon. The abrupt increase of resistance suggests opening of a gap in the energy spectrum. The onset points for the resistance anomaly are plotted in figure 3 as $\log T_c$ versus $1/B$ (Iye *et al.* 1981). As evident from this figure, the onset points can be represented by the following

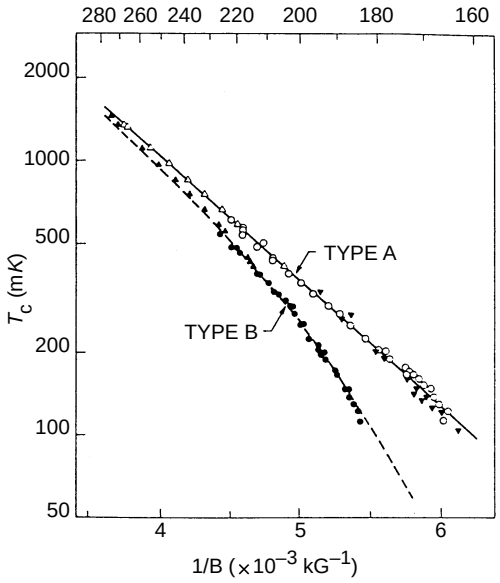

Figure 3. Onset points of the magnetoresistance anomaly plotted as $\log T_c$ versus $1/B$. The straight line for the type-A sample is a fit of equation (2.1). The dashed curve for the type-B sample is a fit of equation (2.4).

empirical formula:

$$T_c = T^* \exp[-B^*/B]. \tag{2.1}$$

Some justification for this functional form is gained by comparing this with the BCS-like formula for a pairing type instability,

$$T_c \approx \varepsilon_F \exp[-1/N(\varepsilon_F)V], \tag{2.2}$$

and by recalling that the density of states at the Fermi level is approximately proportional to B, reflecting the Landau degeneracy factor. By fitting equation (2.1) to the data for the type-A sample in figure 3, we obtain $T^* = 69$ K and $B^* = 105$ T, respectively. This value for the pre-exponential factor is the same order of magnitude as the Fermi energy, $\varepsilon_F \approx 10$ meV. The quantity corresponding to the 'coupling constant', $N(\varepsilon_F)V$, is $B/B^* \approx 0.27$ (at $B = 25$ T), which can be taken as a signature of 'weak-coupling' regime.

Immediately after the first discovery of this phenomenon, Yoshioka & Fukuyama (1981) proposed a theoretical model. Their model is based on an idea that the narrow one-dimensional Landau sub-bands ought to have inherent tendency toward $2k_F$-type instability. There are four spin-split Landau sub-bands crossing the Fermi level, as shown in figure 1. Accordingly, there are many possibilities for the nesting wavevector that connects two Fermi points, and one has to calculate T_c for each one to find the one that gives highest T_c. Yoshioka & Fukuyama's calculation in the Hartree–Fock approximation indicates that the highest T_c occurs for the charge density wave-type instability for the spin-up electron sub-band (the one labelled ($n = 0$, $\sigma = +$) in figure 1) has the highest T_c. The development of charge density wave will open up a gap in the Fermi level and cause a resistivity increase. At the instability point, two mutually out-of-phase charge-density waves originating from the sub-bands located at the H-K-H and H'-K'-H' edges develop. A more proper name for this phase, therefore, may be a valley density wave state. The calculated $T_c(B)$ is similar in

functional form as equation (2.1), and the absolute value is correct order of magnitude with a reasonable choice of the parameter governing the screening of the Coulomb interaction. All of the four spin-split sub-bands have potential instabilities. Which of them has the highest transition temperature is a subtle issue. In fact, other authors have reached different conclusions concerning this point (Sugihara 1984; Takahashi & Takada 1994).

As seen in figure 2, the sharp increase of resistivity at the onset does not continue up to higher magnetic fields. The non-vanishing conductivity indicates that the high-field phase retains some Fermi surfaces. The system may therefore undergo successive phase transitions at higher magnetic fields, as will be discussed later.

(*c*) *Properties of the high-field phase*

In this section, I summarize relatively well-established facts about this phase transition and properties of the high-field phase.

(i) *Tilted magnetic field*

Measurements with tilted magnetic fields have established that only the magnetic field component along the *c*-axis is effective in determining the onset point of the anomaly (Timp *et al.* 1983).

(ii) *Effect of pressure*

An experimental support for the picture explained in the previous section has been obtained from study of pressure effect (Iye *et al.* 1990). Figure 4 shows the phase boundaries in the B-T plane for different values of applied pressure. Application of pressure increases the overlap integral $|\gamma_2|$. In the present pressure range, the change in γ_2 is linear in pressure: $\gamma_2(p) = (1 + \alpha p)\gamma_2(0)$. If we incorporate this pressure dependence into equation (2.1), assuming both T^* (proportional to ε_{F}) and B^* (proportional to $N(\varepsilon_{\mathrm{F}})^{-1} \propto \varepsilon_{\mathrm{F}}$) to be proportional to γ_2, we obtain

$$T_{\mathrm{c}}(B, p) = (1 + \alpha p)T^* \exp[-(1 + \alpha p)B^*/B]. \tag{2.3}$$

The straight lines in figure 4 show fit of this formula with the pressure coefficient $\alpha = \mathrm{d}\ln|\gamma_2|/\mathrm{d}p \approx 0.03\ \mathrm{kbar}^{-1}$. This value of pressure coefficient is within the range of reported values, $0.024 < \mathrm{d}\ln|\gamma_2|/\mathrm{d}p < 0.043\ \mathrm{kbar}^{-1}$.

(iii) *Effect of impurities*

As seen in figure 3, the samples labelled type-B show consistently lower T_{c} than the type-A samples at a given magnetic field (Iye *et al.* 1985). Type B samples contain (unintentionally doped) ionized donors, whose concentration is estimated as $N_{\mathrm{D}}^+ = n - p \approx 2 \times 10^{16}\ \mathrm{cm}^{-3}$ from the carrier density imbalance as determined from the Hall measurement. (If there is compensation, the total concentration, $N_{\mathrm{D}}^+ + N_{\mathrm{A}}^-$, of ionized impurities would be higher.) The suppression of T_{c} is explained by pair-breaking effect of ionized impurity scattering. In fact, the dashed curve in figure 3 is a fit of the formula for T_{c} in the presence of pair breakers,

$$\ln\left(\frac{T_{\mathrm{c}}}{T_{\mathrm{c}0}}\right) = \Psi(\tfrac{1}{2}) - \Psi\left(\tfrac{1}{2} + \frac{\hbar}{2\pi\tau k_{\mathrm{B}} T_{\mathrm{c}}}\right), \tag{2.4}$$

where $T_{\mathrm{c}0}$ is the critical temperature in the absence of pair-breaking effect and $\Psi(x)$ is the digamma function. The scattering time $\tau \approx 6 \times 10^{-11}$ s obtained from the fit is in a reasonable range.

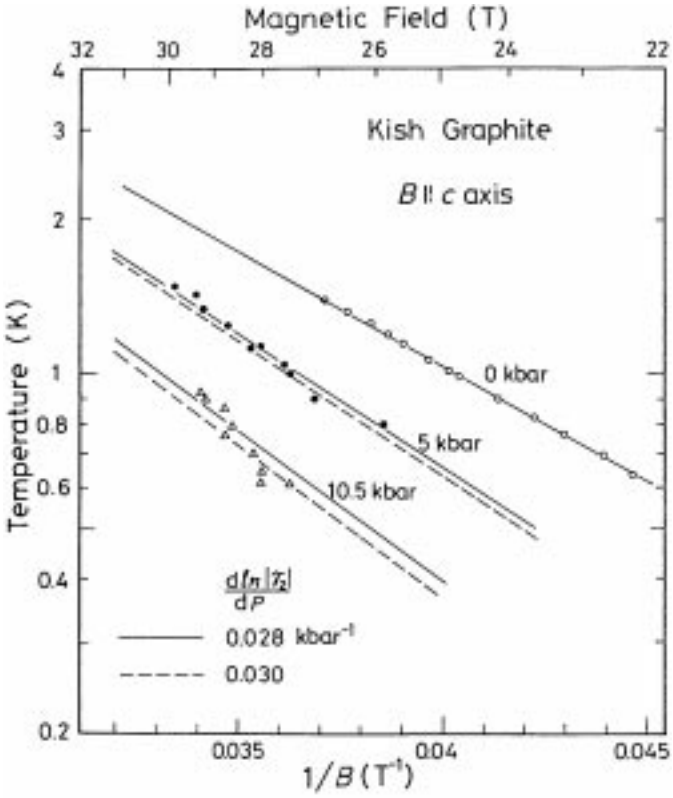

Figure 4. Effect of pressure on the onset points of the resistance anomaly.

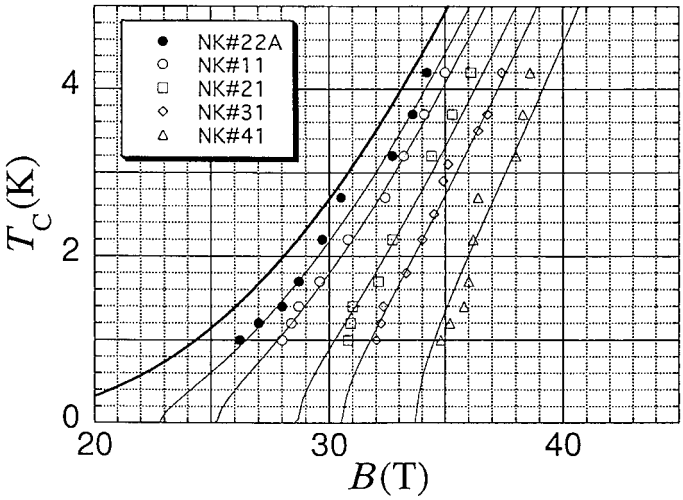

Figure 5. Phase boundaries for neutron-irradiated graphite samples. The curves are fit of equation (2.4).

The pair-breaking effect smears the energy gap, and just below T_c in particular, a gapless state should occur. It is seen in figure 2 that the increase of resistivity above the onset field is more gradual in the type-B sample, which is consistent with the

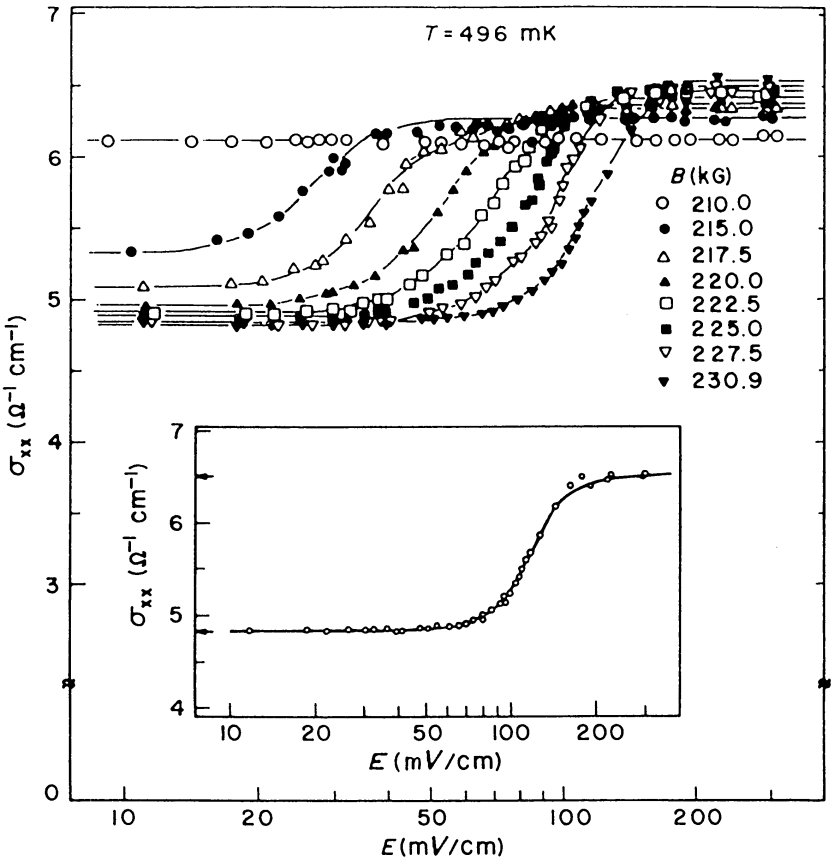

Figure 6. Magnetoconductivity σ_{xx} as a function of electric field at several fixed values of magnetic field, exhibiting non-ohmicity in the high-field phase. The inset shows fit of an empirical functional form.

pair-breaking picture. It should be also noted that the effectiveness of the ionized impurity scattering as a pair-breaker fits to the general picture of charge density wave instablity. Because the charge density wave is caused essentially by electron-hole pairing, scattering by a Coulomb centre which deflects the electron and the hole differently will break the pair.

(iv) *Neutron irradiation*

The ionized impurity concentration of even the type-B sample is too small (less than 0.2%) to shift the Fermi level significantly. Neutron irradiation creates vacancies which act as acceptors and create an imbalance between p and n, which can be determined by the Hall and Shubnikov-de Haas measurements. At the highest neutron dose, $(p-n)/\frac{1}{2}(p+n)$ is about 30%. Since the resulting shift in the Fermi level should have different effects on T_c for different $2k_F$-type instabilities, one may gain information on the nature of the high-field phase. Figure 5 shows T_c versus B for a series of neutron-irradiated samples. The thick curve is the phase boundary for unirradiated samples (Yaguchi *et al.* 1995). The open symbols correspond to four samples with different neutron dosage. The solid circles are the data for a sample irradiated and then heat treated to anneal out the vacancies. Introduction of the ionized acceptors has a side effect, namely pair breaking scattering. It has been found

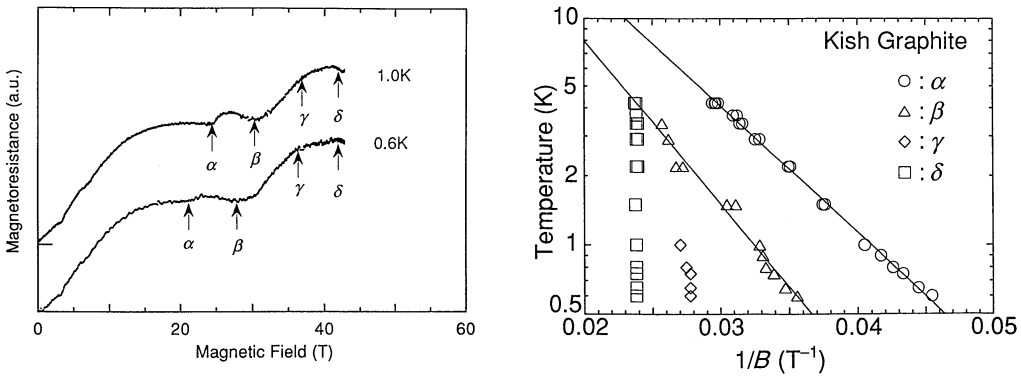

Figure 7. (Left) Magnetoresistance curves measured in pulsed magnetic fields. (Right) The positions of the structures (labelled as α, β, γ and δ on the traces in the left panel) plotted on the plane.

difficult to separate the effect of Fermi level shift and the effect of pair-breaking scattering. In fact, the curves in figure 5 are the fit of equation (2.4) to the experimental data.

(v) *Nonlinear conduction*

Figure 6 shows the conductivity as a function of electric field at fixed magnetic field and temperature (Iye & Dresselhaus 1985). As the system enters the high-field phase, non-ohmicity appears in such a way that the conductivity switches from its low electric field value to a high electric field value at around a threshold field in the range of 20 to 50 mV cm^{-1}. This is reminiscent of nonlinear transport due to depinning of a charge density wave condensate observed, for example, in $NbSe_3$. Here the non-ohmicity appears in the basal-plane transport. This type of nonlinear transport cannot be explained by the aforementioned picture of valley density wave along the c-axis in its simplest form, because then the system retains the translational invariance. The nonlinear basal-plane transport suggests that there is also a charge density modulation along the basal plane, even though the principal mechanism for the phase transition may still be the $2k_F$-type instability in the one-dimensional sub-band. One may imagine a highly anisotropic Wigner crystal-like state. Unlike the case of one-dimensional charge density wave materials such as $NbSe_3$, where a sharp threshold is observed for depinning, the switching from the low to high electric field regime is gradual in the present case. Non-one-dimensional nature of the charge density wave may be responsible for such a gradual depinning. Nonlinear transport is also observed in the vertical transport.

(*d*) *Open questions*

(i) *Anomalies at higher magnetic fields*

Figure 7*a* shows $\rho_{xx}(B)$ measured to higher magnetic fields by use of a pulse magnet (Yaguchi *et al.* 1993). In addition to the magnetoresistance anomaly (labelled α in this figure) which has been discussed above, a few additional structures are discerned in the $\rho_{xx}(B)$ curve. Figure 7*b* shows the onset positions of the anomalies plotted in the T versus B plane; as mentioned before, since there is ample possibility for successive phase transitions. At the moment, identification of the anomalies at higher fields has not been completed.

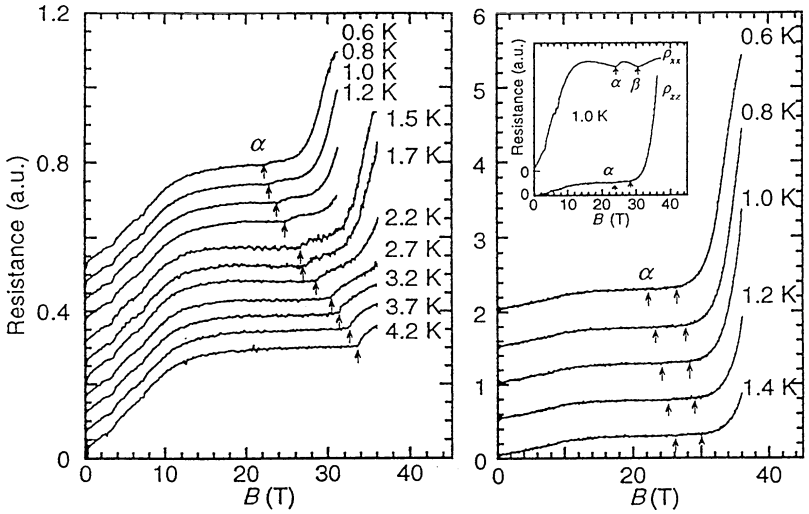

Figure 8. Traces of the c-axis (longitudinal) magnetoresistivity $\rho_{zz}(B)$ at different temperatures. The right panel shows the same data as the left panel. The inset of the right panel compares $\rho_{zz}(B)$ with $\rho_{xx}(B)$.

(ii) *Vertical conduction*

Figure 8 shows the experimental traces of the c-axis resistivity, $\rho_{zz}(B)$ (Yaguchi *et al.* 1997). At the onset, points of the anomaly in the $\rho_{xx}(B)$ (labelled α in figure 7), marked by arrows, $\rho_{zz}(B)$ shows only a small change. The increase of $\rho_{zz}(B)$ starts at a higher magnetic field. Whether it corresponds to the second anomaly (labelled β in figure 7) in $\rho_{xx}(B)$ is not clear at the moment.

(*e*) *Summary*

Although the overall body of accumulated experimental results seem consistent with the general picture of nesting-type instability of magnetic field-generated one-dimensional narrow sub-bands, we are still lacking clear-cut evidence revealing the nature of the high-field phase. Owing to the requirement of high magnetic field and low temperature to reach the high-field phase, experiments to date have been limited to transport measurements. It is important to extend the measurements to a wider range of properties of this high-field phase. It is also a challenge to explore still more phases that possibly await us at higher magnetic fields and lower temperatures.

3. III-V based diluted magnetic semiconductors

(*a*) *Diluted magnetic semiconductors*

Diluted magnetic semiconductors (DMSs) occupy a unique position in semiconductor physics and magnetism (see, for example, Furdyna & Kossut 1988). Traditionally, the main body of research has been focused on II-VI compounds such as (Hg,Mn)Te and (Cd,Mn)Te. The III-V compounds have been more difficult to prepare with high concentrations of magnetic dopants. Recently, growth of (In,Mn)As and (Ga,Mn)As with a few percent Mn content have been achieved by molecular beam epitaxy at low substrate temperature (Munekata *et al.* 1989; Ohno *et al.* 1992). Doped manganese ions act as acceptors. (In,Mn)As and (Ga,Mn)As containing a few percent of Mn have been found to exhibit ferromagnetism at low temperatures. The strong

Table 1. *List of* $Ga_{1-x}Mn_xAs$ *samples*

sample	1	2	3	4	5	6
Mn content, x	0.015	0.022	0.035	0.043	0.055	0.071
conduction	non-metallic	non-metallic	metallic	metallic	non-metallic	non-metallic
magnetism	para.	ferro.	ferro.	ferro.	ferro.	ferro.
Curie point, T_c		5 K	65 K	70 K	50 K	35 K

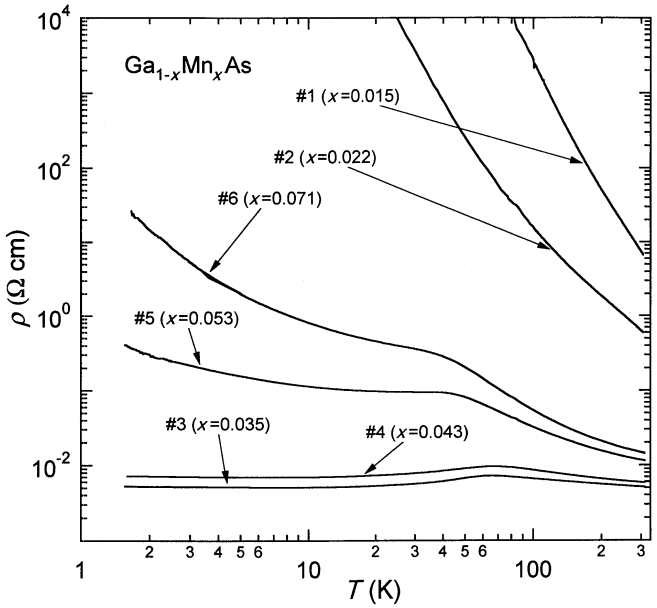

Figure 9. Temperature dependence of the resistivity for six samples of $Ga_{1-x}Mn_xAs$. The numbers in the parenthesis are the Mn content x.

exchange interaction between the hole carriers and localized Mn spins gives rise to dramatic magnetotransport phenomena such as anomalous Hall effect and extremely large negative magnetoresistance. Here, we focus on the (Ga,Mn)As system (Oiwa *et al.* 1997).

(*b*) *Metal–non-metal transition as a function of Mn content*

A series of (Ga,Mn)As samples with different Mn contents were grown on GaAs(100) substrate by molecular beam epitaxy. Growth of a (Ga,Mn)As layer (150 nm thick) was done at *ca.* 250 °C on top of a GaAs buffer layer (100 nm thick). The Mn content x was estimated by electron probe micro-analysis (EPMA). The uncertainty in the value of x was about 10%. The lattice mismatch between (Ga,Mn)As and GaAs causes a compressive strain in the (Ga,Mn)As layer. Six samples used in the present study are listed in table 1.

Let us first look at the overall trend of transport behaviour as a function of the Mn content. Figure 9 shows the temperature dependence of resistivity for the six samples with different Mn contents. Sample 1 with the lowest Mn content ($x = 0.015$) shows an insulating behaviour with an activation energy $\Delta \approx 75$ meV. This value of activation energy is comparable to the value for the ionization energy (*ca.* 110 meV)

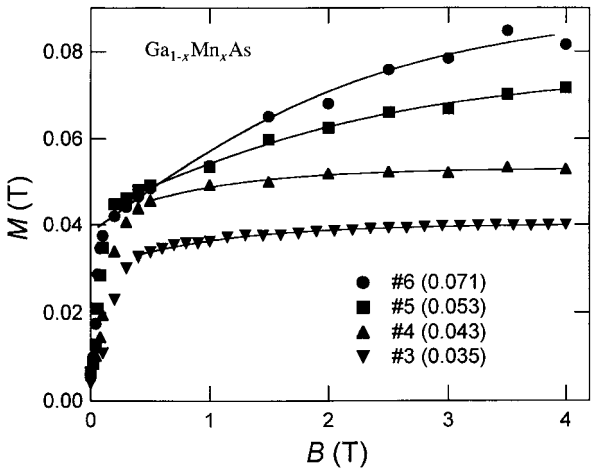

Figure 10. Magnetization curves for four samples of $Ga_{1-x}Mn_xAs$ (from sample 3 to 6) at helium temperature.

of Mn in GaAs given in the literature. Sample 2 ($x = 0.022$) shows a similar $\rho(T)$ with a somewhat reduced activation energy, $\Delta \approx 40$ meV. This sample becomes ferromagnetic at low temperatures ($T_c \approx 5$ K). A non-metal–metal transition occurs in the Mn content range between sample 2 ($x = 0.022$) and 3 ($x = 0.035$). This value for the critical Mn concentration for the non-metal–metal transition is considerably higher than the value ($n_h \approx 2 \times 10^{19}$ cm^{-3}) often quoted in the literature (Edwards & Sienko 1978). However, the authors of the original paper (Woodbury & Blakemore 1973) state that their 'metallic' samples have rather high resistivities and conduction is only through filamentary channels. Or, the difference can be due to the difference between their bulk samples and our epitaxial film samples.

Samples 3 ($x = 0.035$) and 4 ($x = 0.043$) are ferromagnetic metals with $T_c \approx 70$ K. (The values of T_c were determined from the Arrott plot of the magnetization data at different temperatures.) The $\rho(T)$ curve has a peak around T_c. Samples 5 ($x = 0.053$) and 6 ($x = 0.071$) with higher Mn content exhibit semiconductor-like transport behaviour. They are also ferromagnetic with Curie temperature, $T_c = 50$ and 35 K, respectively. The peak in $\rho(T)$ around T_c is also seen in these samples. Thus, with increasing Mn concentrations, the system evolves from a non-magnetic non-metal to a magnetic metal and then to a magnetic non-metal.

(*c*) *Magnetization and magnetotransport*

Figure 10 shows magnetization curves for the four samples (3–6) at helium temperature. In the low-field range ($B < 0.1$ T), these samples exhibit ferromagnetic hysteresis loops, which are not visible in the scale of this figure. In samples 5 and 6, the magnetization curve has a component which increases gradually at higher fields. The values of magnetization to which these curves are tending in the high-field limit are consistent with the saturation magnetization $M_s = N_{Mn} g \mu_B S$ calculated with $g = 2$ and $S = \frac{5}{2}$. Out of all the Mn moments in sample 6, only about 40–50% are aligned at low magnetic fields, and the rest takes much higher fields to align. Such a slowly saturating component, although smaller in fraction, is also present in samples 3 and 4.

Now we turn to the magnetotransport behaviour. We begin with the metallic regime. Figure 11 shows the longitudinal and Hall resistivities in sample 3 at different

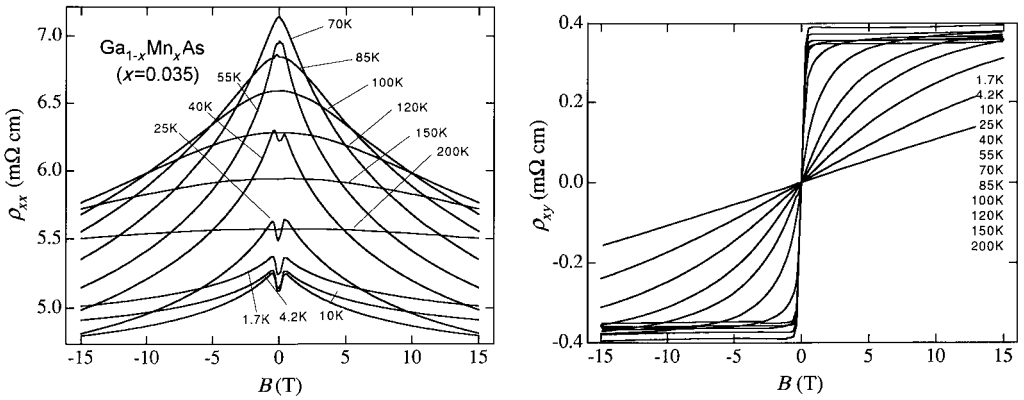

Figure 11. Longitudinal and Hall resistivities in sample 3 ($x = 0.035$) at different temperatures.

temperatures. The Hall resistivity $\rho_{xy}(B)$ can be expressed as

$$\rho_{xy}(B) = R_{\mathrm{H}}^{0} B + R_{\mathrm{S}} M, \tag{3.1}$$

where R_{H}^{0} and R_{S} are ordinary (or normal) and extraordinary (or anomalous) Hall coefficients, respectively. The extraordinary Hall coefficient is related with the resistivity by $R_{\mathrm{S}} \propto \rho$, or $R_{\mathrm{S}} \propto \rho^2$, depending on whether the skew scattering or the side jump is the dominant mechanism to give rise to asymmetric scattering. In figure 11 and for other samples as well, the Hall resistivity is dominated by the extraordinary term. Indeed, R_{S}/ρ (or R_{S}/ρ^2) plotted against B reproduces the magnetization curve quite well. The dominance of the extraordinary term causes difficulty in extracting the carrier density from the ordinary Hall term. Nevertheless, if we naively assume that the slope of $\rho_{xy}(B)$ at the lowest temperature and in the highest magnetic field range is due to the ordinary Hall effect, we obtain $p \approx 6 \times 10^{20}\ \mathrm{cm}^{-3}$ as the hole density in this sample. This is consistent with the picture that the doped Mn ions are in the divalent state and supply a single hole each.

The longitudinal resistivity $\rho_{xx}(B)$ shows a rather complicated T and B dependence. At temperatures below T_{c} and in the low-field range, a small positive magnetoresistance is observed. The salient features of this positive magnetoresistance may be summarized as follows: (i) it is present only in the ferromagnetic phase and the field range of its appearance roughly coincides with the range of ferromagnetic hysteresis loop; (ii) it is sensitive to the magnetic field orientation with respect to the transport current; and (iii) its magnitude is about 1%. From these observations, we attribute this positive magnetoresistance to the so-called anisotropic magnetoresistance effect ubiquitously observed in ferromagnetic materials. Except for the small positive component, the overall magnetoresistance is negative. The negative magnetoresistance becomes largest around T_{c}. The behaviour above and near T_{c} can be basically interpreted in terms of spin-disorder scattering. The fact that the change in the resistivity extends to the field range much higher than the ferromagnetic hysteresis loop suggests that the phenomenon is associated with the slowly saturating component of magnetization, as seen in figure 10.

The negative magnetoresistance becomes very large in the semiconducting samples 5 and 6. Figure 12 shows $\rho_{xx}(B)$ for sample 6. At the lowest temperature ($T = 1.4\ \mathrm{K}$), the resistivity in the high-field range is diminished by more than two orders of magnitude from the zero-field value.

As for the non-metallic samples at lower Mn concentrations, magnetoresistance in

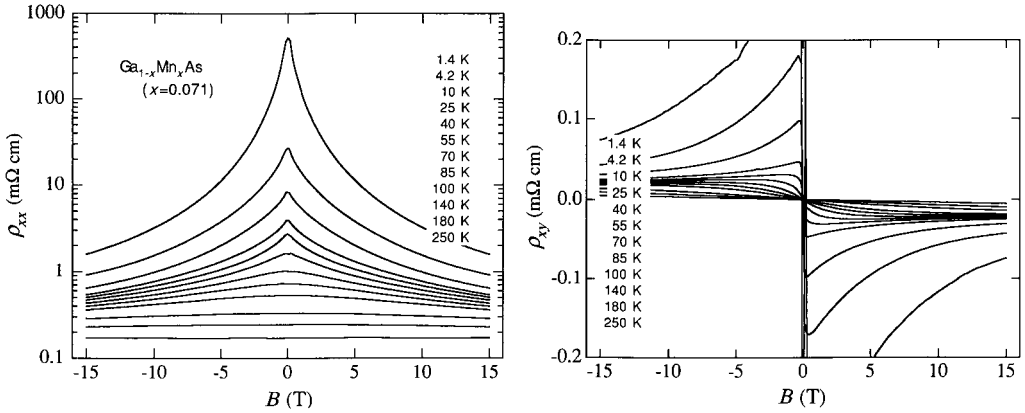

Figure 12. Longitudinal and Hall resistivities in sample 6 ($x = 0.071$) at different temperatures.

sample 1 very small, but sample 2 exhibits negative magnetoresistance comparable to those found in samples 5 and 6. In short, large negative magnetoresistance appears in samples that are located relatively close to the metal–non-metal transition and are fairly resistive.

(*d*) *Models for the negative magnetoresistance*

As seen above, the magnetotransport reflects the coupling of carrier with localized Mn moments. In the metallic regime, relatively mobile holes of density (*ca.* 6×10^{20} cm^{-3}) are scattered by the Mn impurities. The structure in the $\rho(T)$ curve around T_c can be attributed to spin disorder scattering. Analysis of the magnetoresistance data in the paramagnetic region above T_c in terms of the spin disorder scattering model yields a fit with a reasonable value of the coupling parameter between the carrier spin and the localized moment (Matsukura *et al.*, unpublished). On the other hand, the magnetoresistance behaviour at low temperatures is difficult to understand within the same framework, because well below T_c, the change in the magnetization occurs at low fields, as seen in figure 10.

In the semiconducting regime at higher Mn concentrations (samples 5 and 6), holes tend to be localized by disorder. The large negative magnetoresistance seen in figure 12 implies that magnetic field induces carrier delocalization. Since the field range in which the large negative magnetoresistance occurs is much higher than that for the ferromagnetic hysteresis loop, it is natural to associate the carrier delocalization to the slowly saturating component of magnetization. As mentioned earlier, the slowly saturating component or magnetization increases with increasing Mn concentration, while the ferromagnetic component stays roughly constant. The coexistence of these two components is associated with Mn clustering. Namely, a certain fraction of Mn form ferromagnetic clusters, while the rest constitute spin-glass-like random configurations. In samples 5 and 6, the latter component amounts to 50–60%. The holes are strongly localized at zero field and become progressively mobile as the randomly oriented moments are aligned by the applied field.

We consider a few candidate models for the conduction mechanism in the non-metallic samples. One may invoke magnetic polarons, i.e. holes bound to their surrounding cloud of Mn spins polarized by p–d exchange interaction. At zero magnetic field, the magnetic polarons tend to be strongly bound due to their large effective mass. Motion of a magnetic polaron involves realignment of a large number of Mn

moments. Application of high magnetic fields aligns those Mn moments and reduces the polaronic cloud, leading to delocalization of carriers. In this picture, the negative magnetoresistance is attributed to diminishing of the polaronic effect by magnetic field.

Another line of approach is to attribute the large magnetoresistance to change in the localization length. In a strongly Anderson localized system, the Fermi level ε_{F} lies on the localized side of the mobility edge ε_{c}. The conductivity at low temperature is exponentially dependent on the localization length $\xi \propto |\varepsilon_{\mathrm{c}} - \varepsilon_{\mathrm{F}}|^{-\nu}$. Magnetic field changes $|\varepsilon_{\mathrm{c}} - \varepsilon_{\mathrm{F}}|$ to $|\varepsilon_{\mathrm{c}} - \varepsilon_{\mathrm{F}} \pm g\mu_{\mathrm{B}}B|$ by the Zeeman shift. For one of the spin sub-bands, the mobility edge moves toward the Fermi level, while it moves away for the other spin sub-bands. Because of the exponential dependence of the conductivity on the localization length, the former effect dominates the latter and leads to a negative magnetoresistance. This mechanism for negative magnetoresistance was first proposed by Fukuyama & Yosida in the context of negative magnetoresistance observed in TaS_2 (Fukuyama & Yosida 1972).

We expect that a similar phenomenon can occur in diluted magnetic semiconductors even more drastically. Firstly, the Zeeman splitting of the conduction electrons (or holes) will be enhanced by the exchange coupling with the localized moments. Secondly, the mobility edge itself may be a function of magnetic field, if the randomness of the system at zero field comes from spin disorder and is reduced at higher fields. In this case, the relevant localization length depends on magnetic field as $\xi \propto |\varepsilon_{\mathrm{c}}(B) - \varepsilon_{\mathrm{F}} \pm g\mu_{\mathrm{B}}B|^{-\nu}$. If, for example, the main conduction process is variable range hopping, the conductivity is given by $\sigma \propto \exp[-C(T_0/T)^{1/4}]$, where $k_{\mathrm{B}}T_0 \approx 1/N(0)\xi^3$ and ξ is given above. To proceed further, we need to know the functional form of $\varepsilon_{\mathrm{c}}(B)$.

(*e*) *Summary*

In summary, we have observed a non-metal–metal-non-metal transition in the (Ga,Mn)As system as a function of the Mn content. Charge transport in this system is closely linked with magnetism. In particular, a large negative magnetoresistance is found at low temperatures in the semiconducting samples near the metal–non-metal transitions. The phenomenon appears to be correlated with the existence of slowly saturating component of magnetization. We presented two types of models for mechanism of large magnetoresistance. Obviously, further investigation is needed to elucidate the basic mechanism for the intriguing variety of transport and magnetic properties in these DMS.

The work presented in this paper is the fruit of collaborative efforts of my colleagues. I thank, in particular, H. Yaguchi, T. Takamasu, N. Miura, T. Iwata, L. E. McNeil, G. S. Boebinger, P. M. Berglund, J. T. Nicholls, P. M. Tedrow, G. Dresselhaus, M. S. Dresselhaus and L. G. Rubin for the studies of graphite, and A. Oiwa, S. Katsumoto, A. Endo, M. Hirasawa, H. Ohno, F. Matsukura, A. Shen, Y. Sugawara and H. Munekata for the studies of diluted magnetic semiconductors. This work has been supported in part by Grant-in-Aid for Scientific Research, from the Ministry of Education, Science, Sports and Culture.

References

Brandt, N. B., Chudinov, S. M. & Ponomaev, Y. G. 1988 *Semimetals I. Graphite and its compounds*. Amsterdam: North-Holland.

Edwards, P. P. & Sienko, M. J. 1978 *Phys. Rev.* B **17**, 2575.

Fukuyama, H. & Yosida, K. 1972 *J. Phys. Soc. Jap.* **46**, 102.

Furdyna, J. K. & Kossut, J. 1988 *Semiconductor and semimetals*, vol. 25. New York: Academic.

Iye, Y. & Dresselhaus, G. 1985 *Phys. Rev. Lett.* **54**, 1182.

Iye, Y., Tedrow, P. M., Timp, G., Shayegan, M., Dresselhaus, M. S., Furukawa, A. & Tanuma, S. 1982 *Phys. Rev.* B **25**, 5478.

Iye, Y., McNeil, Y. E., Dresselhaus, G., Boebinger, G. S. & Berglund, P. M. 1985 In *Proc. Int. Conf. on the Physics of Semiconductors* (ed. J. D. Chadi & W. A. Harrison), p. 981. Berlin: Springer.

Iye, Y., Murayama, C., Mori, N., Yomo, S., Nicholls, J. T. & Dresselhaus, G. 1990 *Phys. Rev.* B **41**, 3249.

Munekata, H., Ohno, H., von Molnar, S., Segmueller, A., Chang, L. L. & Esaki, L. 1989 *Phys. Rev. Lett.* **63**, 1849.

Ohno, H., Munekata, H., Penny, T., von Molnar, S. & Chang, L. L. 1992 *Phys. Rev. Lett.* **68**, 2664.

Ohno, H., Shen, A., Matsukura, F., Oiwa, A., Endo, A., Katsumoto, S. & Iye, Y. 1996 *Appl. Phys. Lett.* **69**, 363.

Oiwa, A., Katsumo, S., Endo, A., Hirasawa, M., Iye, Y., Ohno, H., Matsukura, F., Shen, A. & Sugawara, Y. 1997 *Solid State Commun.* **103**, 209.

Sugihara, K. 1984 *Phys. Rev.* B **29**, 6722.

Takahashi, K. & Takada, Y. 1994 *Physica* B **201**, 384.

Timp, G., Dresselhaus, P. D., Chieu, T. C., Dresselhaus, G. & Iye, Y. 1983 *Phys. Rev.* B **28**, 7393.

Woodbury, D. A. & Blakemore, J. S. 1973 *Phys. Rev.* B **8**, 3803.

Yaguchi, H., Iye, Y., Takamasu, T. & Miura, N. 1993 *Physica* B **184**, 332.

Yaguchi, H., Takamasu, T., Iye, Y. & Miura, N. 1995 In *Proc. 11th Int. Conf. on Application of High Magnetic Fields in Semiconductor Physics* (ed. D. Heiman). Singapore: World Scientific. p. 742.

Yoshioka, D. & Fukuyama, H. 1981 *J. Phys. Soc. Jap.* **50**, 725.

Discussion

C. N. R. Rao (*Indian Institute of Science, Bangalore, India*). (1) Did Dr Iye try to intercalate graphite (say with alkali metals)?

(2) Is GMR greater at the M–SC transition than at the I–M transition in the manganate semiconductors? Even in the manganates, GMR is higher when the resisitivity at the I–M transition is higher.

(3) Is there Mn^{2+} ion clustering at high Mn doping? This may give rise to unusual magnetic effects (e.g. AFM interactions).

Y. Iye. (1) Upon intercalation, the Fermi energy usually changes by 0.1–1 eV, and the system becomes a metal with carrier density on the order of 10^{21} cm^{-3}. That would make a totally different situation. What we wish to do here is to change the Fermi level (and hence the carrier density) by a small amount, so that we can still reach the quantum limit within the accessible magnetic range.

(2) The magnetoresistance is small in sample 1, with the lowest Mn concentration. However, fairly large negative magnetoresistance is observed in sample 2 which is closer to the non-metal transition. In short, large negative magnetoresistance is observed in samples that are relatively close to the metal–non-metal transition, and are fairly resistive.

(3) Yes, we do believe there is considerable clustering of Mn ions, particularly at higher doping. Such spatially inhomogeneous Mn ions may form a mixture of ferromagnetic clusters and spin glass-like regions. The latter is presumuably responsible for the slowly saturating component of the magnetization.

R. McGreevy (*Studsvik Neutron Research Laboratory, Sweden*). A common mistake when considering doping of materials is to confuse 'random' doping with 'uniform' doping. Random doping, even at low concentrations like 5%, will lead to significant numbers of clusters whose interactions may dominate the magnetic behaviour. It is only necessary to change the Mn distribution away from random by a very small amount to significantly vary the connectivity of clusters and hence T_c.

Y. Iye. I completely agree. The drawing on one of my transparencies you refer to was no more than a sketch and by no means intended to claim uniform distribution.

P. P. Edwards (*School of Chemistry, University of Birmingham, UK*). Is it possible to probe the evolution of Mn^{2+} clustering via EPR measurements?

Y. Iye. I believe one can, in principle, gain information of Mn ions from EPR measurements, as done in the case of phosphorous doped silicon, for example. I am not aware of any such study done on the present system. I know too little about the EPR experiment to judge if there would be any practical difficulties in carrying out such experiments.

W. J. Nellis (*Lawrence Livermore Laboratory, University of California, USA*). Is it possible that in Mn alloys, local moments rather than Mn moments are favoured at lower Mn concentrations and that local magnetic moments transform to itinerant band moments at higher Mn concentrations? The transition from local to itinerant magnetic moments might open up a gap in the band structure. Is it possible that Mn magnetization is caused by Mn ferrimagnetism, i.e. a combination of ferro- and antiferromagnetism?

Y. Iye. As for the possibility of itinerant magnetism, I believe it is unlikely because the magnetization data in the paramagnetic phase above T_c are fully consistent with that of local moments.

If you use the term ferrimagnetism in the textbook sense, it does not apply to the present case. If you mean, instead, a mixture of ferro and antiferromagnetism, that is exactly the picture we have. We believe that the magnetism is caused by combinations of ferromagnetic clusters and more or less antiferromagnetically coupled groups of moments. The fraction of Mn moments that participate in the latter increases as we go towards the higher Mn concentrations.

D. P. Tunstall (*School of Physics and Astronomy, University of St Andrews, UK*). Does Dr Iye believe that any of the transitions he observed at high field in graphite related to the Wigner crystallization?

Y. Iye. Yes. We may call the high field state a sort of anisotropic Wigner crystal.